Journal of Biomolecular NMR, **15:** 39–53, 1999.
KLUWER/ESCOM

NMR structure determination of the tetramerization domain of the Mnt repressor: An asymmetric α-helical assembly in slow exchange

Irene M.A. Nooren[a], Albert V.E. George[a], Robert Kaptein[a], Robert T. Sauer[b] & Rolf Boelens[a,*]
[a]*Department of NMR Spectroscopy, Bijvoet Center for Biomolecular Research, Utrecht University, Padualaan 8, 3584 CH Utrecht, The Netherlands*
[b]*Department of Biology, Massachusetts Institute of Technology, Cambridge, MA 02139, U.S.A.*

Received 3 May 1999; Accepted 7 July 1999

Key words: asymmetry, homotetramer, inter-subunit NOE, protein structure, slow chemical exchange

Abstract

The structure and dynamics of the chymotryptic tetramerization domain of the Mnt repressor of *Salmonella* bacteriophage P22 have been studied by NMR spectroscopy. Two sets of resonances (A and B) were found, representing the asymmetry within the homotetramer. Triple-resonance techniques were used to obtain unambiguous assignments of the A and B resonances. Intra-monomeric NOEs, which were distinguished from the inter-monomeric NOEs by exploiting $^{13}C/^{15}N$-filtered NOE experiments, demonstrated a continuous α-helix of approximately seven turns for both the A and B monomers. The asymmetry facilitated the interpretation of inter-subunit NOEs, whereas the antiparallel alignment of the subunits allowed further discrimination of inter-monomeric NOEs. The three-dimensional structure revealed an unusual asymmetric packing of a dimer of two antiparallel right-handed intertwined coiled α-helices. The A and B forms exchange on a timescale of seconds by a mechanism that probably involves a relative sliding of the two coiled coils. The amide proton solvent exchange rates demonstrate a stable tetrameric structure. The essential role of Tyr 78 in oligomerization of Mnt, found by previous mutagenesis studies, can be explained by the many hydrophobic and hydrogen bonding interactions that this residue participates in with adjacent monomers.

Introduction

Together with the homologous Arc repressor, the Mnt repressor of *Salmonella* bacteriophage P22 regulates the switch between the lysogenic and lytic pathways in the genetic immunity I region of the phage (Susskind and Youderian, 1983). Mnt maintains lysogeny by repression of the transcription of the *arc* and *antirepressor* genes during the lysogenic state of the prophage, while Arc represses Mnt and antirepressor as well as its own synthesis during lytic phage growth. Arc repressor occurs predominantly as a dimer and forms a tetramer upon operator binding, whereas Mnt repressor is already tetrameric in solution (Vershon et al., 1985). Structure determination of symmetric oligomeric proteins by NMR spectroscopy presents a problem, since the degenerate chemical shifts of each monomer do not allow to distinguish between intra- and inter-monomer NOE signals. The first symmetric homodimeric proteins for which the structures were solved by NMR spectroscopy were interleukin-8 (Clore et al., 1990) and the Arc repressor (Breg et al., 1990). For the Arc repressor the intra- and inter-subunit connectivities could be distinguished based on homology modeling of the MetJ repressor (Breg et al., 1990), which together with the Arc and Mnt repressors belongs to the β-sheet DNA-binding family (Knight et al., 1989). The structure elucidation of many other symmetric dimers followed, using isotope

*To whom correspondence should be addressed. E-mail: boelens@nmr.chem.uu.nl
Supplementary material available from the corresponding author on request: (1) Gel filtration chromatogram of the mixture of cleaved Mnt-C and uncleaved wild-type Mnt repressor on a Superdex HR30 under denaturating conditions, (2) Table listing the unique set of NOEs used to model the four-helix bundle orientation as demonstrated in Figure 3.

filtered experiments in combination with asymmetric labeling, and simulated annealing methods dealing with the ambiguity of intra- and inter-monomer NOEs (for review see O'Donoghue and Nilges, 1999). Only for a few higher order oligomers has the structure been solved by NMR, demonstrating the difficulties in interpretation of NOE data introduced by symmetry.

The N-terminal part (1–51) of the tetrameric Mnt repressor has been characterized as the dimerization and DNA-binding region and is homologous to the 53-residue Arc repressor, whereas the C-terminal domain (52–82), which is lacking in Arc, is involved in tetramerization (Waldburger and Sauer, 1995). In fact, C-terminal deletion studies demonstrated that Tyr 78 plays a key role in tetramerization, since the Mnt (1–77) mutant loses the ability to form stable tetramers (Knight and Sauer, 1988). The solution structure of the dimeric Mnt (1–76) mutant revealed an Arc-like tertiary structure for the N-terminal dimerization domain, forming an intermonomeric antiparallel β-sheet and closely arranged α-helices (Burgering et al., 1994). For the truncated C-terminal region, an unstable third helix from residue 53 to 66 was found, followed by an unstructured peptide tail (Burgering et al., 1994). The N- and C-terminal domain of the wild-type repressor protein can be separated by a chymotryptic cleavage at the carboxyl side of Tyr 51 (Waldburger and Sauer, 1995). Although helical formation was also clear from CD studies on the C-terminal fragment (residues 52–82), structural data on how tetramerization of Mnt is realized was not available.

Recently, we have determined the three-dimensional structure of the tetramerization domain of the Mnt repressor by NMR spectroscopy on the C-terminal chymotryptic fragment of Mnt, referred to as Mnt-C (Nooren et al., 1999). The present paper describes in detail the methodology used for the structure determination of Mnt-C. The Mnt-C peptide forms tetramers under NMR conditions as judged from cross-linking experiments (Waldburger and Sauer, 1995). The structure consists of a dimer of two anti-parallel right-handed coiled coils that assemble as a four-helix bundle with C_2 symmetry. The right-handed supercoiling in the intertwined coiled-coil structure differs from the left-handed coiled coils as observed in leucine zippers and fibrous proteins. An asymmetry within the homotetramer exists between the subunits that comprise one coiled coil and a slow exchange process between these asymmetric subunits is observed. Two sets of NMR resonances represent the asymmetric assembly of the four subunits. This was clearly advantageous for the interpretation of inter-subunit NOEs. Next to isotope filtered experiments and structure calculation strategies using symmetric ambiguous distance restraints, the rigid α-helical structure of the monomer restricted the quarternary assembly of the four subunits satisfying the inter-subunit NOE data. A highly resolved structure was obtained that allows to explain the essential role of Tyr 78 in tetramerization of the Mnt repressor.

Materials and methods

Protein purification and sample preparation

As described by Milla et al. (1993) the His-tagged wild-type Mnt repressor (Mnt-st6) was expressed in *E. coli* strain X90 (Amman et al., 1983) transformed with plasmid pTM203-st6 plasmid (Waldburger and Sauer, 1995). To obtain isotope enrichment with ^{15}N and/or ^{13}C, cells were grown on minimal media with addition of 0.5 g/l $^{15}NH_4Cl$ and/or 2 g/l ^{13}C-glucose, respectively. A 10% ^{13}C labelled Mnt-st6 was prepared by using 10% ^{13}C-glucose and 90% ^{12}C-glucose as the sole carbon source (Neri et al., 1989). The Mnt-st6 protein was purified from the cell lysate by Ni affinity chromatography followed by CM-Accell cation exchange, as described previously with only minor revisions (Milla et al., 1993; Waldburger and Sauer, 1995). For the Ni-NTA superflow column (Qiagen), a step elution of 20 mM and 200 mM imidazole was performed. The Mnt-st6 fraction elutes at 200 mM imidazole. The equilibration buffer contained 3 mM imidazole in 6 M guanidine hydrochloride, 100 mM KPi (pH 8) and 10 mM Tris-HCl (pH 8). Solubility during the renaturation step was improved by addition of 50 mM KCl and 5% glycerol to the dialysis buffer.

The C-terminal Mnt fragment was obtained by cleavage of the Mnt-st6 by chymotrypsin at the carboxyl side of Tyr 51 (Waldburger and Sauer, 1995). The enzymatic reaction was performed in 10 mM Tris-HCl (pH 7.6) and 250 mM KCl at a protein concentration of 0.8–1.2 mg/ml. An enzyme–substrate ratio of 1:500 resulted in high yields of the Mnt-C fragment and low aspecific cleavage. After 30 to 45 min of incubation, the reaction was stopped by addition of 0.2 mM PMSF and 2.5% β-mercapto-ethanol. To avoid formation of heterodimers or -tetramers between uncleaved Mnt-st6, the N-terminal (Mnt-N) and C-terminal (Mnt-C) fragments, further purification steps were performed under denaturing conditions: 100 mM KPi (pH 8), 10 mM Tris-HCl (pH 8) and 6 M guani-

dine hydrochloride. Ni-affinity chromotography was used to separate Mnt-N from the His-tagged Mnt-C and wild-type protein. FPLC gel filtration using a Superdex HR30 column (Pharmacia) gave a good separation of Mnt-C and Mnt-st6 (Supplementary material).

The purified Mnt-C peptide was renaturated by dialysis against water or 100 mM ammonium bicarbonate and lyophilized. The dry Mnt-C fragment was dissolved in a 50 mM KPi, 200 mM NaCl, pH 5.2 buffer. For all samples, 0.01% Na-azide was added to prevent bacterial growth. Also, 2 mM Pefabloc, 1 μM leupeptine and 1 mM EDTA were added to inhibit residual protease activity. An isotopically mixed tetramer was obtained by a 1:1 mixture of unlabeled ($^{14}N/^{12}C$) and $^{15}N/^{13}C$-labelled Mnt-C. For the lock, 5% D_2O was used in all H_2O samples.

NMR measurements

NMR experiments were recorded on Bruker AMXT-600 and Varian Unity Plus 750 spectrometers, both equipped with a triple resonance gradient probe. The NMR spectra used for the structure determination of Mnt-C were measured at 25 °C. ^1H, ^{15}N and ^{13}C heteronuclear correlation spectra that were used for backbone (3D TOCSY-(^{15}N,^1H)-HSQC, 3DNOESY-(^{15}N,^1H)-HSQC, 3D HNCO, 3D HNCA, 3D HNHA, 3D HN(CO)CA, 3D HCACO) and side-chain (3D TOCSY-(^{13}C,^1H)-HSQC, 3D HNHB, 3D H(C)CH-DIPSY, 3D HCC(H)-DIPSY) assignments were performed as described earlier (Vis et al., 1994; Fogh et al., 1995). Also, homonuclear clean-TOCSY spectra with a mixing time of 30–90 ms (Bothner-By et al., 1984; Griesinger et al., 1988) and NOESY spectra with a mixing time of 25–100 ms were used (Jeener et al., 1979). Stereo-specific assignments of the methyl protons in the pro-chiral centre of all leucines and valines were obtained from a 10% ^{13}C labelled sample of Mnt-C as described by Neri et al. (1989). Several β-methylene protons could be stereo-specifically assigned by analysis of the 3D HNHB experiment (Düx et al., 1997) in combination with a TOCSY, recorded with a mixing time of 30 ms. The chemical shifts of Mnt-C have been deposited in the BioMagnetic Resonance Bank with accession number 4355.

Chemical exchange was measured using ROESY (Bothner-By et al., 1984; Bax and Davis, 1985) experiments, recorded at different temperatures and with a mixing time of 50–100 ms. ^{13}C double-half filtered 2D and 3D NOE experiments served to discriminate intra- and intersubunit NOEs between the symmetric monomers (Burgering et al., 1993; Folkers et al., 1993; Slijper et al., 1996; Zwahlen et al., 1997). Hydrogen-deuterium exchange rates were measured by dissolving the lyophilized protonated protein in D_2O with an adjustment to pD 5.2 and recording a series of short (^{15}N,^1H)-HSQC spectra, where the first experiment was started 9 min after dissolving. Heteronuclear ^{15}N-^1H-NOE measurements were recorded at 600 MHz based on the sequence as described earlier (Dayie and Wagner, 1994; Vis et al., 1998). All spectra were processed with the NMRPipe package (Delaglio et al., 1993) and analyzed using the program REGINE (Kleywegt et al., 1993). In-house developed software was used to analyze the relaxation and H-D exchange data according to Vis et al. (1998).

Structure calculations and analysis

Interproton NOE distance restraints were derived from a NOESY with a mixing time of 60 ms and a 3D NOESY-(^{15}N,^1H)-HSQC and NOESY-(^{13}C,^1H)-HSQC with a 75 ms mixing time. Using secondary structure elements for calibration, peak volumes obtained from 2D spectra and intensities obtained from 3D NOESY spectra were translated into distance restraints by grouping them into three distance ranges, 1.8–2.8 Å, 1.8–3.5 Å and 1.8–5.5 Å, corresponding to strong, medium and weak NOEs. Pseudo-atom corrections were added for distances that involved aromatic ring protons and non-stereo-specifically assigned methylene protons, according to the method of Wüthrich (1986), while 0.3 Å was added for the methyl groups (Koning et al., 1990). Hydrogen bonds were implemented for slowly exchanging amides by using a distance restraint of 1.7–2.5 Å between the corresponding carbonyl oxygen and amide proton and 2.3–3.5 Å between the carboxyl oxygen and amide nitrogen. Additional experimental input was provided by ϕ and χ_1 dihedral restraints, obtained from a 3D HNHA and HNHB experiment, respectively. To maintain the symmetry of the A and B monomers, which followed from the chemical shift data, the XPLOR non-crystallographic symmetry (ncs) term (Brünger, 1992) and pseudo-NOE distance restraints as described by Nilges (1993) were used. The A_1 and A_2subunits comprised one and the B_1 and B_2 subunits another ncs group.

From randomized atomic coordinates, structures were calculated using the program XPLOR-3.851 (Brünger, 1992). The initial ensemble of 30 structures was generated using a restrained dynamical simulated annealing protocol in cartesian coordinate

space (Nilges et al., 1988). Subsequently, iterations were performed decreasing the number of ambiguous intra- or inter-subunit NOE distance restraints (Nilges, 1993). For the final ensemble, a selection was made based on low total energy criteria. The final set of 27 structures were analysed using XPLOR and the software program PROCHECK (Laskowski et al., 1993). This ensemble has been deposited in the Protein Data Bank (accession number 1QEY). Molecular figures were prepared using the program MOLMOL (Koradi et al., 1996).

Results and discussion

NMR assignments: Two sets of resonances

Mnt-C was prepared by chymotryptic cleavage of the wild-type Mnt repressor protein and purification under denaturating conditions (see Methods). Using the *E. coli* expression system of the wild-type Mnt protein allowed for the necessary isotope enrichment of the peptide under study. A close examination of the (^{15}N,^{1}H)-HSQC spectrum and other NMR spectra of Mnt-C reveals a doubling of NMR resonances. The two sets of resonances represent two different conformations of the peptide. As will be shown below, NOEs are observed between the two sets of resonances. Hence, this phenomenon was attributed to asymmetry within the homotetramer, rather than two co-existing tetrameric structures. Equal intensities of resonances indicate that the two sets of resonances, labeled A and B, originate from two symmetric monomers A and two symmetric monomers B, respectively. Besides the regular sequence-specific assignments, the resonances of the asymmetric Mnt-C tetramerization domain required A/B-specific assignments that were obtained using triple-resonance techniques.

3D HNCA and 3D HN(CO)CA experiments on ^{13}C/^{15}N enriched Mnt-C peptide were exploited to construct two continuous sequential-assignment walks through the peptide chain. In case of overlap between the A and B resonances in the carbon dimension, the HN-HN (i,i+1) NOE contacts in the 3D NOESY-(^{15}N,^{1}H)-HSQC permitted the A/B-specific sequential assignment of the backbone resonances. Other triple resonance experiments (HNCO, HCACO, HNHA) and a 3D TOCSY-(^{15}N,^{1}H)-HSQC were used to obtain carbonyl and Hα resonance assignments. From the unambiguous sequential assignments of backbone resonances, the side-chain assignments were obtained from a set of 3D HCCH-DIPSI experiments and a 3D TOCSY-(^{15}N,^{1}H)-HSQC. Overlap of the A and B backbone resonances only occurs for the N-terminal residue Arg 52. For this residue, A/B-specific side-chain resonance assignments could be performed using sequential connectivities in the 2D NOESY. All ^{1}H, ^{15}N and ^{13}C resonances were unambiguously assigned for both asymmetric subunits (Table 1), except for the Cβ of Ser 63-A and 63-B, Cβ and Cγ of Gln 62-B and Cβ of Tyr 78-A. Line broadening of the resonances of these carbon-attached protons indicated chemical exchange on the millisecond timescale. Three resonances corresponding to exchangeable protons could be observed, that were assigned to the hydroxyl protons of Ser 63-A, Ser 63-B and Tyr 78-A, based on a 2D TOCSY and short-range NOE connectivities. The signal detection of the hydroxyl protons that normally exchange rapidly with the bulk water implies involvement in strong hydrogen bonding.

The chemical shifts of Mnt-C resemble those of the tetramerization domain in the wild-type Mnt repressor and infer native structural properties. This includes the observation of the solvent exchangeable side-chain protons (unpublished results).

The asymmetric A and B subunits exchange

Many of the A/B-specific resonances show rather large differences in chemical shift (Table 1), indicating a considerable asymmetry between the A and B segments. The dashed lines in the assigned (^{15}N,^{1}H)-HSQC spectrum of Mnt-C show this for the amide resonances connecting the A and B signals of each residue (Figure 1a). A comparison of the NOE patterns at the A and B resonances of one particular proton demonstrates the difference in chemical environments of the A and B peptides. Figure 1b shows the A/B-specific NOE patterns of the aromatic protons of Tyr 78, that is known to be essential for tetramer formation of the Mnt repressor. The hydroxyl signal that is observed for Tyr 78-A, but not for Tyr 78-B, and the larger number of NOEs observed for the Tyr 78-A aromatic protons suggest a closer packing of the Tyr 78-A side chain.

As judged from the one-to-one ratio of the A and B signals, it is equally probable for an Mnt-C monomer to adopt the A or B conformation. Several NMR experiments revealed that the two conformations slowly interconvert. As shown for the Tyr 78 aromatic resonances, clear positive cross peaks between the A and B resonances in a 2D ROE spectrum, recorded at 35 °C with a ROE mixing time of 75 ms, indicate chemical exchange between the A and B conformations

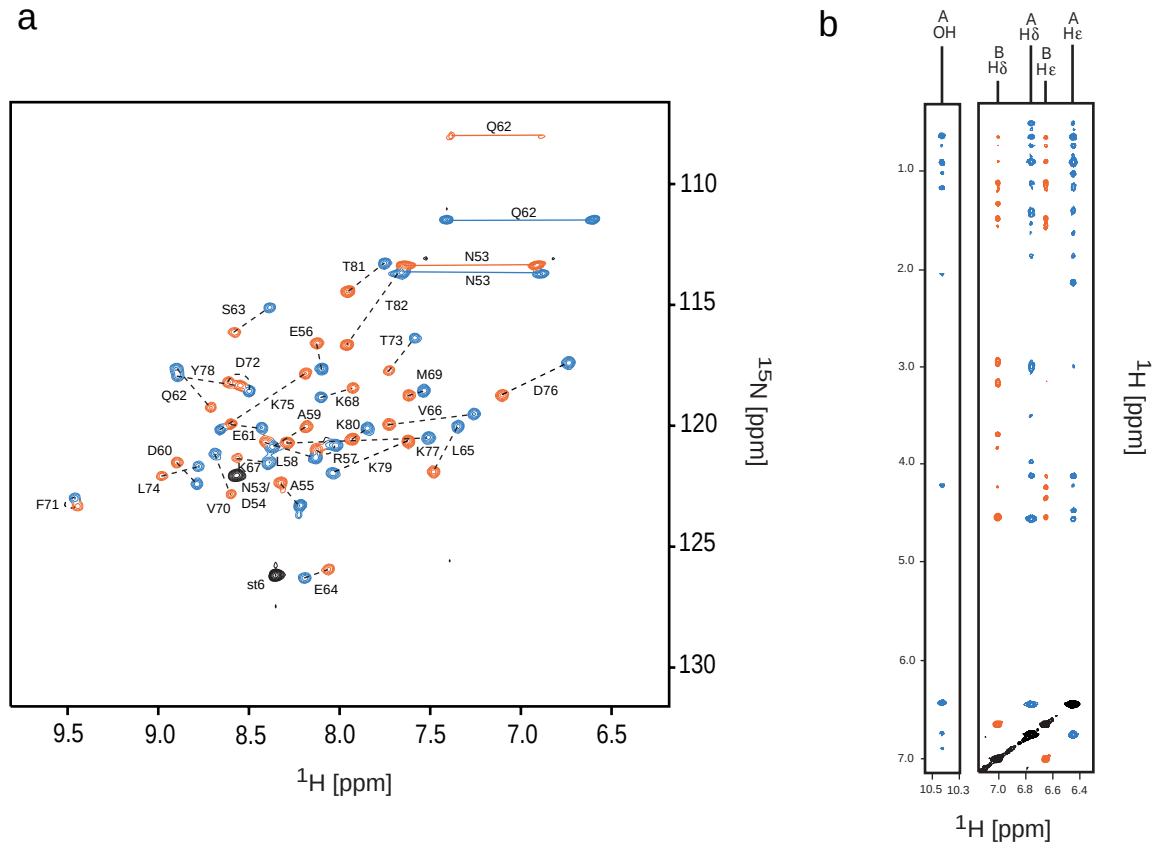

Figure 1. (a) Assigned (^{15}N,^{1}H)-HSQC spectrum of Mnt-C. The dashed lines connect the A and B amide cross peaks for every residue, as depicted in blue and orange, respectively. (b) Part of the aromatic region of the 2D NOESY in D_2O (right panel) and part of the 2D NOESY in H_2O (left panel) at the F2 frequency of the Tyr 78 aromatic protons and Tyr 78-A hydroxyl proton respectively, showing the difference in NOE patterns of the Tyr 78-A and Tyr 78-B aromatic protons.

(Figure 2a). A 3D TOCSY-(^{15}N,^{1}H)-HSQC experiment recorded at 35 °C with a mixing time of 60 ms displayed exchange cross peaks as well between the A and B proton resonances of all amides. Figure 2b shows the nitrogen planes of this 3D spectrum for the A and B amide resonances of Asp 76. The exchange cross peaks confirmed the sequence-specific assignments by connecting the A/B-specific resonances. The same experiments at different temperatures indicated a strong temperature dependence of the rate of interconversion. At 25 °C the exchange process is slowed down to such an extent that during mixing times of up to 75 ms no significant build up of exchange cross peak intensity takes place (Figure 2c,d). At 35 °C and 500 MHz, an intermediate exchange regime is reached if the specific A and B resonances have only a small difference in chemical shift. From the observed line-broadening of the proton amide signal of Phe 71 and the chemical exchange cross peak intensities, the exchange rate could be estimated to be approximately 1 s^{-1} at 35 °C and slower than 0.1 s^{-1} at 25 °C.

Interpretation of intersubunit NOE

The NOEs used for the structure determination were collected from a 2D NOESY, 3D NOESY-(^{15}N,^{1}H)-HSQC and 3D NOESY-(^{13}C,^{1}H)-HSQC, recorded at 25 °C with mixing times of 60, 75 and 75 ms, respectively. As pointed out above, the A↔B chemical exchange contribution for NOE mixing times up to 75 ms is negligible at 25 °C. The asymmetry of the Mnt-C homotetramer, fully denoted as $A_1A_2B_1B_2$, facilitated the identification of intra- or inter-subunit NOEs to a certain extent. As compared to a fully symmetric tetramer, the number of possibilities is decreased significantly because NOEs that originate from the A and B type monomers can be distinguished directly by their difference in chemical shift. For the symmetric subunits of the tetramer, we used 2D ^{13}C/^{15}N-

Table 1. NMR resonance assignments of Mnt-C at 25 °C and pH 5.0[a]

Residue	N	HN	C	Cα	Hα	Cβ	Hβ	Cγ	Hγ	Cδ	Hδ	Others
R52-A	–	–	–	53.4	4.13	29.4	1.94, 1.94	24.5	1.71, 1.71	41.8	3.18, 3.18	Nε: 84.9, Hε: 7.51
R52-B	–	–	–	53.4	4.13	29.4	1.94, 1.94	24.5	1.72, 1.72	41.8	3.19, 3.19	Nε: 84.9, Hε: 7.53
N53-A	122.1	8.60	173.0	50.8	4.83	37.1	2.94, 3.03	–	–	–	–	Nδ2: 113.7, Hδ21: 7.65, Hδ22: 6.92
N53-B	122.1	8.59	173.0	50.8	4.83	37.1	2.93, 3.03	–	–	–	–	Nδ2: 113.4, Hδ21: 7.70, Hδ22: 6.90
D54-A	122.1	8.58	173.0	54.7	4.41	38.9	2.65, 2.65	–	–	–	–	–
D54-B	122.1	8.60	173.0	55.1	4.42	38.9	2.62, 2.62	–	–	–	–	–
A55-A	123.3	8.24	175.1	53.1	3.83	16.9	1.32	–	–	–	–	–
A55-B	122.4	8.33	175.0	53.7	3.97	17.0	1.44	–	–	–	–	–
E56-A	117.7	8.11	177.2	57.7	3.88	27.9	2.18, 2.18	35.4	2.31, 2.47	–	–	–
E56-B	116.6	8.13	176.9	58.0	3.86	27.9	2.18, 2.18	35.7	2.36, 2.45	–	–	–
R57-A	120.8	8.05	176.3	57.5	4.12	28.3	1.97, 1.87	25.4	1.75, 1.59	41.5	3.28, 3.20	Nε: 83.8, Hε: 7.39
R57-B	121.0	8.15	176.1	57.7	4.13	28.3	2.02, 1.85	25.4	1.74, 1.59	41.4	3.31, 3.19	Nε: 107.7, Hε: 7.41
L58-A	121.3	8.15	176.8	55.8	4.14	39.7	1.54, 1.54	25.1	1.57	22.3*, 22.3*	0.73*, 0.64*	-
L58-B	120.7	8.44	176.7	55.8	4.11	41.3	1.85, 1.38	25.4	1.62	22.9*, 21.7*	0.56*, 0.73*	-
A59-A	120.9	8.39	176.9	52.7	4.33	17.2	1.47	–	–	–	–	–
A59-B	120.1	8.19	176.9	53.3	4.11	17.4	1.39	–	–	–	–	–
D60-A	122.4	8.81	179.2	56.0	4.28	40.0	3.02, 2.96	–	–	–	–	–
D60-B	121.5	8.92	178.6	55.9	4.40	40.0	3.03, 3.03	–	–	–	–	–
E61-A	120.1	8.45	175.6	57.6	3.99	27.8	2.30, 2.14	34.0	2.57, 2.30	–	–	–
E61-B	119.9	8.63	176.1	57.5	4.01	27.8	2.28, 2.14	33.9	2.40, 2.58	–	–	–
Q62-A	117.6	8.92	178.3	56.7	4.16	34.1	2.25, 2.02	32.8	2.50, 2.68	–	–	Nε2: 111.5, Hε21: 6.62, Hε22: 7.44
Q62-B	119.3	8.73	178.4	57.6	4.09	?	2.16, 1.99	33.2	2.65, 3.01	–	–	Nε2: 107.6, Hε21: 7.41, Hε22: 6.91
S63-A	115.1	8.41	177.5	60.5	4.06	?	4.46, 4.11	–	5.64	–	–	–
S63-B	116.1	8.59	177.0	60.7	4.05	?	4.47, 4.12	–	5.56	–	–	–
E64-A	126.3	8.21	174.6	56.6	4.13	27.9	2.11, 2.10	32.7	2.29, 2.40	–	–	–
E64-B	125.9	8.09	174.5	56.6	4.23	–	2.11*, 2.18*	32.7	2.34, 2.40	–	–	–
L65-A	120.0	7.36	176.3	56.2	4.16	39.5	2.03, 1.69	25.0	1.88	23.3*, 21.6*	0.99*, 0.92*	–
L65-B	121.9	7.51	176.6	56.4	4.18	39.6	2.09, 1.72	25.1	1.92	23.8*, 21.7*	1.02*, 0.93*	–
V66-A	119.5	7.27	178.4	64.5	3.67	29.6	2.12	19.9*, 21.0*	0.89*, 0.99*	–	–	–
V66-B	119.9	7.76	178.5	64.6	3.66	29.4	2.23	19.8*, 21.9*	0.87*, 1.07*	–	–	–
K67-A	121.5	8.41	175.1	58.5	3.72	30.7	1.82, 2.23	23.1	1.23, 1.40	27.6	1.61, 1.61	Cε: 41.0, Hε1: 2.87, Hε2: 2.85
K67-B	121.4	8.59	174.7	58.5	3.72	30.7	1.87, 2.26	23.1	1.35, 1.35	27.6	1.62, 1.62	Cε: 40.9, Hε1: 2.85, Hε2: 2.90
K68-A	118.8	8.12	175.7	57.6	4.14	30.7	1.98, 1.98	23.4	1.67, 1.48	27.2	1.81, 1.68	Cε: 40.6, Hε1: 3.04, Hε2: 3.04
K68-B	118.4	7.94	175.7	57.6	4.12	30.7	1.96, 2.01	23.4	1.67, 1.48	27.2	1.81, 1.68	Cε: 40.6, Hε1: 3.05, Hε2: 3.05
M69-A	118.6	7.55	175.7	57.0	4.28	31.3	2.27, 2.29	29.8	2.48, 2.80	–	–	Cε: 15.1, Hε: 2.06
M69-B	118.7	7.63	175.5	56.9	4.29	32.0	2.24, 2.38	29.1	2.67, 2.40	–	–	Cε: 15.1, Hε: 2.05
V70-A	121.1	8.69	177.8	65.2	3.43	29.7	2.14	19.8*, 22.1*	0.84*, 1.00*	–	–	–
V70-B	122.8	8.59	177.2	63.4	4.21	30.6	2.12	19.8*, 21.7*	1.02*, 1.17*	–	–	–
F71-A	123.0	9.48	174.6	60.1	4.03	37.3	3.21, 3.43	–	–	–	7.20	Hε: 7.45, Hζ: 7.33
F71-B	123.3	9.45	175.5	59.8	4.12	37.8	3.30, 3.46	–	–	–	7.22	Hε: 7.48, Hζ: 7.35
D72-A	118.6	8.53	174.3	55.5	4.02	38.1	2.79, 2.64	–	–	–	–	–
D72-B	118.2	8.63	174.7	55.3	4.12	38.1	2.82, 2.63	–	–	–	–	–

Table 1. (Continued)

Residue	N	HN	C	Cα	Hα	Cβ	Hβ	Cγ	Hγ	Cδ	Hδ	Others
T73-A	116.3	7.60	177.0	64.7	3.91	67.0	4.12	19.4	1.17	–	–	–
T73-B	117.7	7.74	177.2	64.9	3.79	66.4	4.46	19.9	0.64	–	–	–
L74-A	121.7	8.79	174.6	55.3	3.50	38.5	1.61, 1.61	24.5	1.86	24.1*, 20.6*	0.91*, 0.63*	–
L74-B	122.1	9.00	174.1	55.9	3.70	40.3	2.00, 2.00	25.2	2.13	26.8*, 21.1*	1.14*, 0.89*	–
K75-A	120.2	8.68	175.3	58.1	3.50	28.9	1.14*, 1.25*	22.8	1.03, 1.23	27.9	1.30, 1.47	Cε: 40.0, Hε1: 2.82, Hε2: 2.76
K75-B	117.8	8.20	176.1	58.4	3.68	29.6	1.50, 1.50	23.2	1.17, 1.12	27.9	1.44, 1.37	Cε: 39.7, Hε1: 2.53, Hε2: 2.79
D76-A	117.4	6.74	175.5	54.8	4.37	39.4	2.61, 2.64	–	–	–	–	–
D76-B	118.7	7.12	176.4	55.0	4.42	39.1	2.68, 2.74	–	–	–	–	–
L77-A	120.5	7.53	175.7	55.5	4.07	41.0	1.42, 1.49	25.1	1.52	21.9*, 23.6*	0.84*, 0.73*	–
L77-B	120.7	8.31	176.6	55.6	3.96	40.0	1.63*, 1.27*	24.5	1.65	24.0*, 20.4*	0.51*, 0.64*	–
Y78-A	117.9	8.90	177.8	54.4	4.55	?	2.96, 3.00	–	–	–	6.75	Hε: 6.44, OH: 10.43
Y78-B	118.3	8.55	178.3	57.0	4.53	?	3.15*, 2.94*	–	–	–	6.99	Hε: 6.64
K79-A	122.0	8.02	176.6	57.0	4.09	30.7	1.92, 1.92	23.7	1.57, 1.46	27.8	1.68, 1.68	Cε: 40.2, Hε1: 2.97, Hε2: 2.97
K79-B	120.6	7.64	175.9	56.0	4.20	30.7	1.96, 1.96	23.4	1.49, 1.61	27.6	1.71, 1.71	Cε: 40.4, Hε1: 2.98, Hε2: 2.98
K80-A	120.1	7.88	176.1	56.3	4.19	30.8	1.96, 1.96	23.4	1.48, 1.60	27.6	1.71, 1.67	Cε: 40.4, Hε1: 2.97, Hε2: 2.97
K80-B	120.6	7.97	175.3	55.2	4.27	30.9	1.88, 1.90	23.3	1.47, 1.55	27.4	1.66, 1.67	Cε: 40.0, Hε1: 2.93, Hε2: 2.93
T81-A	113.3	7.78	176.0	61.9	4.23	67.4	4.11	20.0	1.11	–	–	–
T81-B	114.4	7.97	175.2	60.0	4.39	67.7	4.24	19.8	1.19	–	–	–
T82-A	113.7	7.69	173.0	60.2	4.29	67.7	4.23	20.1	1.18	–	–	–
T82-B	116.7	7.97	172.6	59.9	4.27	67.6	4.12	19.8	1.09	–	–	–

[a]Proton, nitrogen and carbon chemical shifts are referenced to internal H_2O (4.77 ppm) and external $^{15}NH_4Cl$ (^{15}N, 22.3 ppm) and ^{13}C-glucose (^{13}C, 27.8 ppm), respectively. The asterisks denote stereospecific assignment of two nuclei at their prochiral centre, listed in the order proR, proS. Question marks indicate non-assigned resonances. The chemical shifts of Mnt-C have been deposited at the BioMagnetic Resonance Bank (accession number 4355).

filtered NOESY and 3D ^{13}C-filtered NOESY-HSQC experiments on an equimolar mixture of unlabelled ($^{12}C/^{14}N$) and labelled ($^{13}C/^{15}N$) Mnt-C to discriminate the intra-A from inter-A (i.e. between A_1 and A_2) and intra-B from inter-B (i.e. between B_1 and B_2) NOEs. At this stage, however, ambiguity remains for the assignment of the NOEs between the A and B resonances that can arise from close proximity of either the A_1 and B_1 or A_1 and B_2 subunits. Because contacts are inter-subunit in both cases, the filtered NOE spectra did not resolve this problem. Several unique NOEs, however, revealed the subunit arrangement that allowed this discrimination to be made.

From the intra-monomeric sequential and medium-range NOEs, a continuous α-helical structure for both the A and B monomers could be inferred; this is consistent with previous NMR (Burgering et al., 1994) and CD studies (Waldburger and Sauer, 1995). The observation of inter-monomer NOEs between 62-A and 77-A therefore indicated anti-parallel packing of the two A_1 and A_2 α-helices (Figure 3, I). In a similar way, an anti-parallel alignment of the two B_1 and B_2 α-helices could be deduced from inter-monomer NOEs between 55-B and 77-B (Figure 3, II). Further, unique NOEs between A and B resonances could be identified that allowed the arrangement of all four α-helices with respect to each other to be established. In the first place, numerous NOEs were found between the C-terminal region of A and the N-terminal end of B, for example between 78-A and 55-B, 58-B and 59-B. These were defined as contacts between the A_1 and B_1 and, by symmetry, between the A_2 and B_2 subunits (Figure 3, III). Secondly, 78-A also exhibits NOEs to residues 73, 74 and 77 in the C-terminal part of B, which from steric considerations must correspond to close distances between the other combination of A

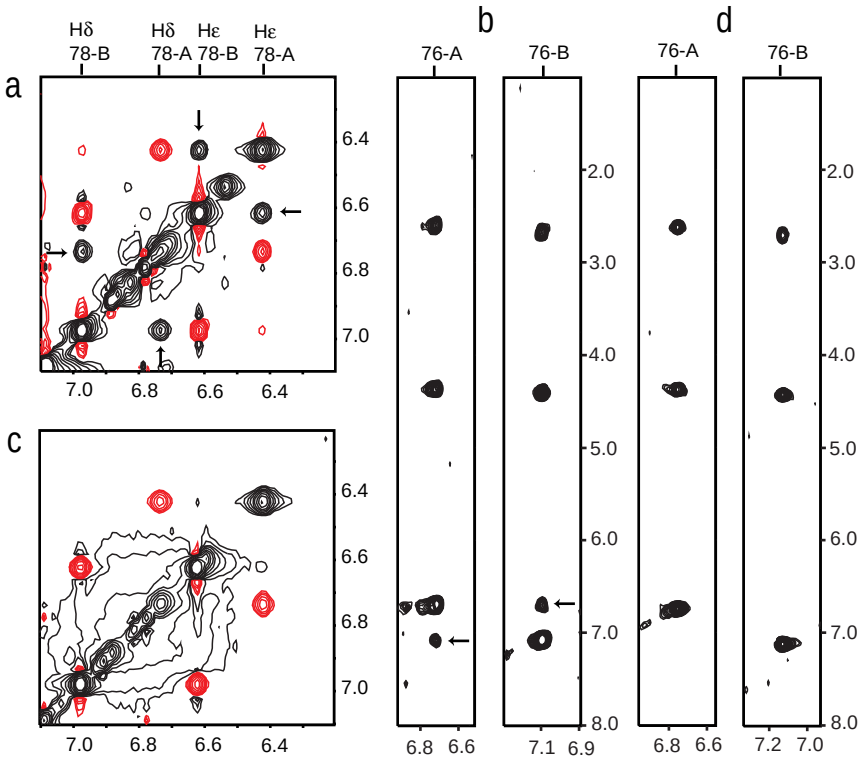

Figure 2. (a,c) Part of the aromatic region in a 2D ROESY experiment ($\tau_m = 75$ ms) showing the Tyr 78 resonances and cross peaks at 35 °C (a) and 25 °C (c). Negative (ROE) peaks are depicted in red. (b,d) Strips from the 3D TOCSY-(^{15}N,^{1}H)-HSQC ($\tau_m = 60$ ms) at the A and B amide resonance frequency of D76 at 35 °C (b) and 25 °C (d), respectively. The arrows indicate the exchange cross peaks.

and B subunits, i.e. A_1 and B_2 or A_2 and B_1, respectively (Figure 3, IV). Subsequently, the unique NOEs between the N-terminal residues 55, 58 and 59 of A and 78-B only fit between the A_1 and B_1 or A_2 and B_2 subunits (Figure 3, V). Thus, the four α-helices can only be arranged as depicted in Figure 3 to satisfy the NOE sets I to V. The A_1 and B_1 helices are anti-parallel whereas A_1 and B_2 run parallel. Likewise, the A_2 and B_2 helices run anti-parallel and the A_2 and B_1 helices parallel. These alignments were crucial for the further assignment of the NOEs.

Structure generation

In the first step of the structure elucidation of Mnt-C, all NOEs corresponding to residues close to the symmetry axis (i.e., in the middle of the helices) were treated as ambiguous (Nilges, 1993). Some of these could be explicitly assigned following iterative structure calculations, others were left ambiguous. Per monomer A or B, the final set of NOE interactions led to a total of 545 intra-A, 501 intra-B, 28 inter A_1-A_2, 16 inter B_1-B_2, 187 A_1-B_1, 69 A_1-B_2 and 49 intra- or inter-ambiguous NOE distance restraints. Additional experimental input was provided by 27 and 26 dihedral angle restraints on ϕ, 3 and 4 dihedral restraints on χ_1 and 44 and 44 hydrogen-bond distance restraints (representing 22 hydrogen bonds for each chain), per A and B monomer, respectively. Slow exchange of the backbone amide protons of residues 57 to 79 with the solvent indicated a stable secondary structure (see Section *dynamical properties*). Symmetry restraints were used to maintain the symmetry between the A subunits and between the B subunits. A simulated annealing protocol was used to generate a family of 30 structures starting from random coordinates. From the 30 structures, 27 were selected according to low energy and low number of NOE violations. The final ensemble (PDB entry 1QEY) has a well-defined core region with a backbone coordinate precision of 0.25 Å to the average (cf. Figure 4). A summary of the structural statistics of the ensemble is given in Table 2. Only very small deviations are found for the used distance restraints, while no violations occur above 0.5 Å. The secondary structure of the all α-helical

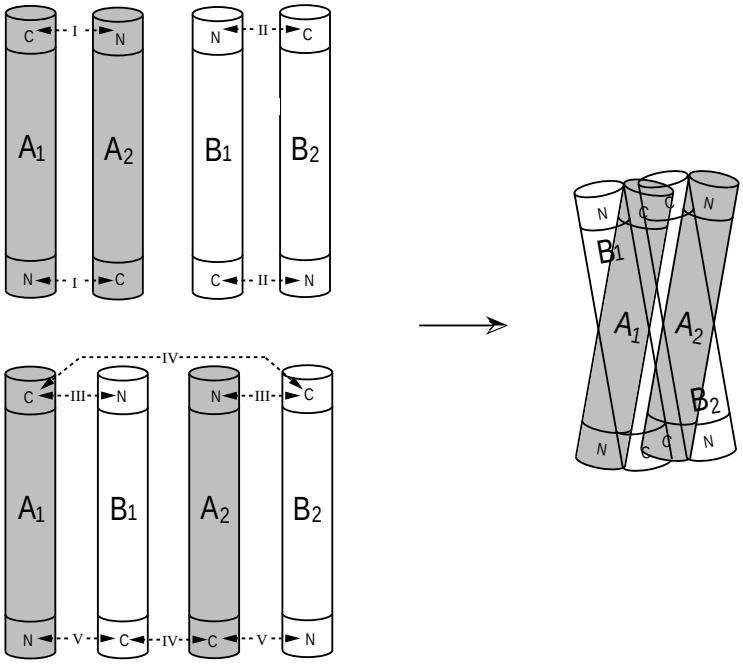

Figure 3. Representation of the A_1, A_2, B_1 and B_2 α-helices and the unique inter-A or inter-B (top left) and inter-AB subunit NOEs (bottom left) that are indicated by dashed arrows and numbered as described in the text (see also supplementary material). The sole arrangement of helices that satisfies these contacts is shown on the right. Based on this simple modeling, right- or left-handedness of the packing is still ambiguous.

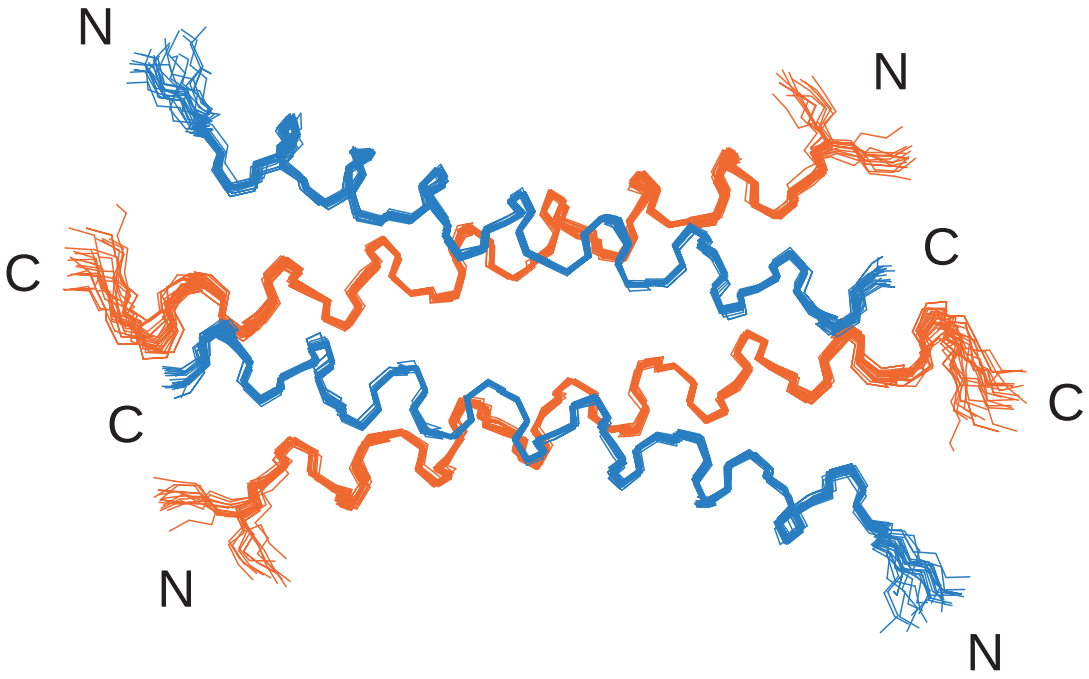

Figure 4. Superposition (residues 57-A to 79-A, 57-B to 78-B) of the backbone atoms of the Mnt-C tetramer in the ensemble of 27 structures (PDB-entry 1QEY). The blue and orange colours indicate the A and B subunits, respectively.

Table 2. Structural statistics of the Mnt-C ensemble

Structural statistics	<SA>[a]
Rms deviations from experimental distance restraints (Å)[b]	
All ($A_1/A_2 + B_1/B_2$: 1439)	0.008±0.001
Intra-monomer[c]	
Intra-residue (A_1/A_2: 221, B_1/B_2: 232)	0.010±0.001
Sequential ($\|i - j\| = 1$) (A_1/A_2: 139, B_1/B_2: 117)	0.009±0.001
Short/medium range ($1 < \|i - j\| \leq 5$) (A_1/A_2: 185, B_1/B_2: 152)	0.007±0.001
H-bonds (A_1/A_2: 22, B_1/B_2: 22)	0.005±0.001
Inter-monomer	
Intra-coiled-coil A_1-B_1/A_2-B_2(187)	0.003±0.001
Inter-coiled-coil A_1-A_2/A_2-A_1(28)	0.002±0.001
Inter-coiled-coil B_1-B_2/B_2-B_1(16)	0.008±0.002
Inter-coiled-coil A_1-B_2/A_2-B_1(69)	0.003±0.001
Ambiguous (A_1/A_2-A_1/A_2(22), B_1/B_2-B_1/B_2(23), A_1/A_2-B_1/B_2(4))	0.001±0.0001
Rms deviations from experimental dihedral restraints (A_1/A_2: 30, B_1/B_2: 30) (°)	0.006±0.012
Deviations from idealized geometry	
Bonds (Å)	0.003±0.0001
Angles (°)	0.360±0.003
Impropers (°)	0.129±0.007
Rms deviations of atomic coordinates of residues 57–79 of A and 57–78 of B (Å)	
Backbone residues	0.25±0.05
All heavy atoms	0.79±0.07
Only core heavy atoms (Ala, Leu, Met, Tyr, Val)	0.44±0.08
Ramachandran plot (% of all residues 54–81 of A and 54–79 of B)	
Most favoured region	97.3±0.1
Additional allowed regions	2.7±0.1
Generally allowed or disallowed regions	0.0±0.0

[a] <SA> are the final 27 simulated annealing structures.
[b] None of the structures exhibited distance violations greater than 0.5 Å and dihedral angle violations greater than 5°. Between brackets the number of restraints are given per monomer A or B.
[c] All long-range restraints are classified in the inter-monomer restraints category.

protein assembly is very well defined according to the Ramachandran plot.

Description of the structure

Residues 54-A to 81-A and 54-B to 79-B display α-helical secondary structure according to the DSSP program (Kabsch and Sander, 1983), each comprising approximately seven helical turns. The quarternary structure of the Mnt tetramerization domain is characterized by a compact and unique four-helix bundle. Interhelical distances and angles are summarized in Table 3. The symmetry of the anti-parallel packed A_1 and A_2 subunits and anti-parallel packed B_1 and B_2 subunits is defined by a common twofold symmetry axis, as depicted in Figure 5a. The asymmetry of the A and B monomers arises from differences between the A_1-A_2 and B_1-B_2 interfaces (Figure 5b). With respect to the relative alignment of the A_1 and A_2 helices, the relative alignment of the B_1 and B_2 helices is shifted by exactly two helical turns (i.e. one helical turn for each helix). For the A_1 and A_2 helices the twofold axis is near Met 69, whereas between the B_1 and B_2 helices the symmetry axis is located near Leu 65. Both the A_1 and A_2 helices and the B_1 and B_2 helices cross at an angle of approximately 160° (Table 3). This so-called 'quasi symmetrical' arrangement of chemically identical subunits, establishing different interface contacts, is unusual in small multimeric systems but has been observed more frequently in large systems such as spherical viruses (Schulz and Schirmer, 1979). As compared to other oligomeric four-helix bundles, such as the oligomerization domains of the tumor suppressor p53 (Lee et al., 1994; Clore et al., 1995) and the *E. coli* lac repressor (Friedman et al., 1995), it differs both with respect to symmetry and handedness of helical packing (Nooren et al., 1999).

Table 3. Interhelical separations and angles[a]

Distance / Angle	A_1	B_1	A_2	B_2
A_1	–	8.0	10.9	9.0
B_1	147	–	9.0	10.5
A_2	161	−15	–	8.0
B_2	−15	159	147	–

[a]Interhelical distances (above the diagonal) represent the closest approach interhelical separations. Interhelical angles (below the diagonal) are given between the two helix vectors according to the convention described by Chothia et al. (1981). The helical axes were determined with the Cα atoms of the residues that comprise the helices. The dssp program (Kabsch and Sander,1983) was used to identify the residues in the α-helices.

Besides symmetry, the topology of the four-helix bundle is determined by the intertwined supercoiling of the asymmetric A and B α-helices (Figure 5c,d). Two-stranded coiled coils of identical subunits have so far only been reported with a left-handed twist as in dimeric leucine zippers or fibrous proteins (Lupas, 1996; Kohn et al., 1997). The Mnt-C tetramer, however, features right-handed coiled coils as described in more detail in Nooren et al. (1999). Typically, the superhelical winding in Mnt-C is stronger and the separation between the supercoiled helices is considerably smaller. Also, while parallel helix pairing is central in the traditional oligomeric coiled coils, in Mnt-C coiled coiling occurs between anti-parallel arranged helices with a crossing angle of approximately 147 °C (Table 3). The interhelical packing within the coiled coil is very compact, as illustrated by interhelical distances as close as 8.0 Å. Both the distribution of the unambiguous inter-monomer NOEs and interhelical distances (Table 3) demonstrate that most of the interactions between the four helices are intra-coiled coil, i.e. within the A_1B_1 or A_2B_2 assembly. The helix interface between the A_1 and A_2 subunits and between the B_1 and B_2 subunits appears to be less compact and confirms a dimer of dimer type of oligomerization in line with chemical cross-linking experiments (Waldburger and Sauer, 1995).

Hydrophobic residues are positioned in the interior and charged residues on the outside of the four-helix bundle of Mnt-C. The packing of the four monomers is mainly hydrophobic, but polar interactions are also part of the interior of the four-helix bundle. The NMR spectra indicated hydrogen bonding of the hydroxyl protons of both Ser 63-A and 63-B, and Tyr 78-A. For the hydroxyl protons of the serine of both the A and B monomer the backbone carbonyl oxygen in the preceding turn of the helix, i.e. of 59, is the most likely hydrogen bond acceptor. This type of intrahelical hydrogen bonding has been reported to have a stabilizing effect on helix formation (Gray and Matthews, 1984). Other electrostatic interactions within the four-helix bundle are mediated by Tyr 78 (see below).

Role of tyrosine 78 in tetramerization

Mutagenesis data on the wild-type Mnt repressor had revealed the crucial role of Tyr 78 in the tetrameric oligomerization state of Mnt (Knight and Sauer, 1988). Its structural basis can now be deduced from its position in the spatial structure of the Mnt-C tetramerization domain. Tyrosine 78 is situated in the C-terminal end of the α-helical monomers and contributes to both intra- and inter-coiled-coil interactions. Within the coiled coils, hydrophobic interactions of the tyrosine ring with the methyl groups of Ala 55, Leu 58 and Ala 59 of its coiled-coil partner are found for both Tyr 78-A and Tyr 78-B. At both terminal ends of the coiled coils, the helices are therefore closely packed. While these interactions are similar in the A and B subunits, the inter-coiled-coil interactions are asymmetric as verified by the difference in the A_1-A_2 and B_1-B_2 interfaces (Figure 5b). The aromatic ring of Tyr 78-A is more buried in the core of the tetramer than that of Tyr 78-B (Figures 1b, 5a). The hydroxyl proton of the buried Tyr 78-A shows slow exchange with water and is therefore suggested to be involved in strong hydrogen bonding. The hydroxyl proton of its asymmetric partner Tyr 78-B exchanges rapidly with water and is more exposed to the solvent.

A detailed view of the close packing of Tyr 78-A is given in Figure 6. Besides the intra-monomeric and intra-coiled-coil contacts, Tyr 78-A_1 mediates several hydrophobic inter-coiled-coil interactions with residues in the B_2 helix (i.e., Val 70, Thr 73, Leu 74 and Leu 77) and by symmetry Tyr 78-A_2 interacts with the B_1 helix. From the side-chain conformations in the ensemble of structures, the hydroxyl oxygen of Thr 73-B_2 of the other coiled coil is likely to serve as hydrogen-bond acceptor of the OH proton of Tyr 78-A_1. For a small percentage of the structures, the amine group of Gln 62-B_1 forms an additional hydrogen bond donor that illustrates a possible bifurcated hydrogen bonding of the hydroxyl proton of Tyr 78-A. In conclusion, the many hydrophobic interactions and hydrogen bonding of Tyr 78 to adjacent

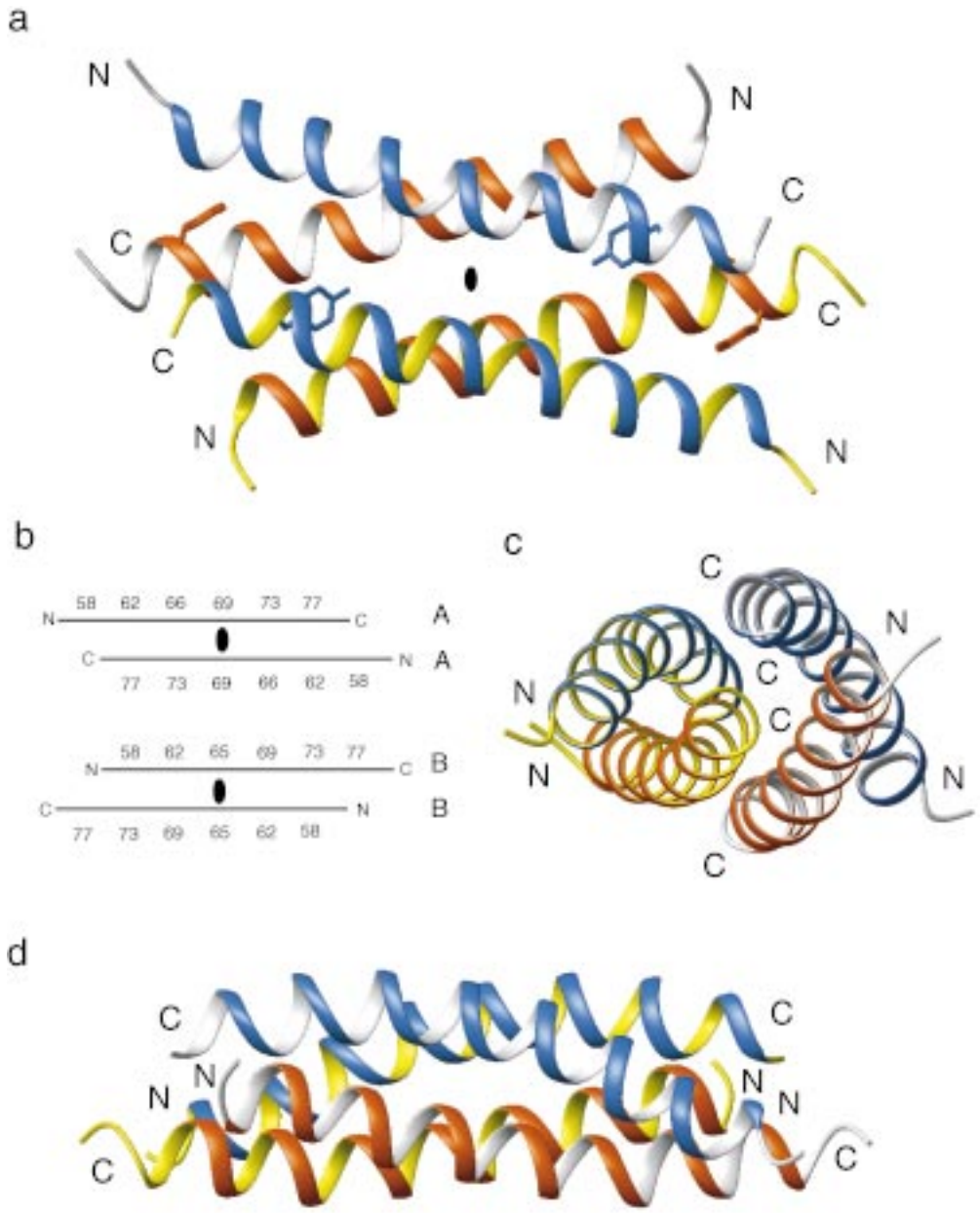

Figure 5. (a) Ribbon diagram of the Mnt-C four-helix bundle illustrating the subunit symmetry. The view is the same as in Figure 5 and depicts the Tyr 78-A and Tyr 78-B side chains (only heavy atoms). The position of the twofold symmetry axis is indicated. (b) Schematic representation of the A_1-A_2 and B_1-B_2 interface. The interface residues and the C_2 symmetry axis are indicated. (c,d) Ribbon diagrams illustrating the intertwined supercoiling of the A and B subunits. The view in (c) is taken along the supercoil axis of one of the coiled coils. In all ribbon diagrams, the same color coding is used: the blue and orange colors on the outside of the ribbon indicate the A and B subunits, respectively, while the two coiled coils are colored white and yellow at the inner side of the helices.

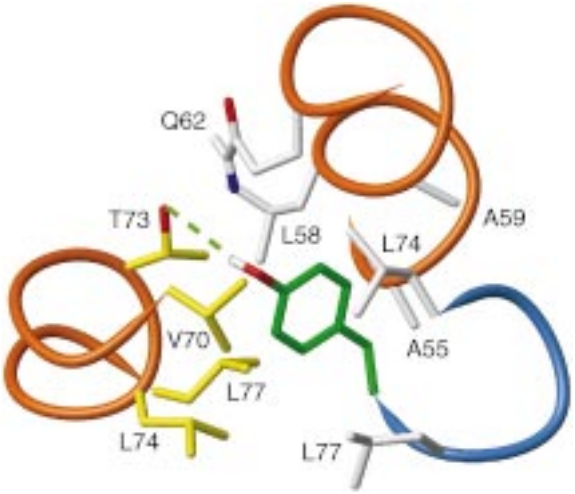

Figure 6. Detailed view of the close packing of Tyr 78-A (in green) to side chains within the same coiled coil (white) or the other coiled coil (yellow). The ribbons of the helices are colored blue for the A and orange for the B subunits. Heavy side chain atoms and the hydroxyl proton of Tyr 78-A are displayed. Oxygens are colored red and nitrogens blue. The hydrogen bond between Tyr78-A and Thr73-B is indicated by a dashed line.

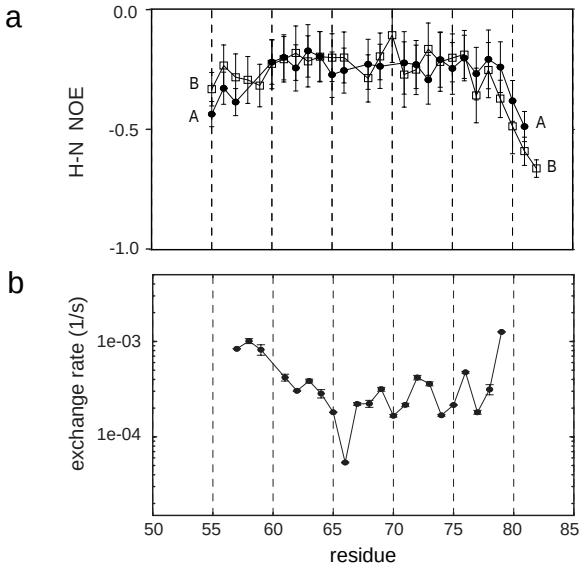

Figure 7. (a) ^{1}H-^{15}N heteronuclear NOE of the backbone amide nitrogens of the A (filled circles) and B (open squares) monomers. Due to A↔B exchange the A and B NOEs could be partly averaged out. (b) Average hydrogen–deuterium exchange rates of the A and B monomers of Mnt-C.

monomers within and between the coiled coils explain its essential role in tetramer formation.

Dynamical properties

The disorder of the N- and C-terminal regions in the ensemble of structures (Figure 4) can be attributed to high backbone flexibility, as supported by ^{1}H-^{15}N heteronuclear NOE data (Figure 7a). In line with the structural disorder, the asymmetric assembly of the helices (Figure 5b) gives rise to a higher backbone mobility at the C-terminus of the B monomers than of the A monomers, while the A monomers have a slightly higher flexibility at the N-terminus. The amide hydrogen–deuterium exchange data (Figure 7b) are consistent with the relaxation data. Due to the chemical exchange between the A and B forms during the recording of the set of HSQC spectra, the slow hydrogen–deuterium exchange rates measured at both the A and B amide resonances represent an average over A and B. From the slow average exchange rates found for residues 57 to 79 (i.e., slower than approximately 10^{-3} s^{-1}) stable hydrogen bonds for both A and B α-helices could be concluded. Consistent in the A and B helices, the amide protons are positioned toward the solvent or protein interior. The average exchange rates reveal a sequential pattern that corresponds well with the helical periodicity and packing (Figure 7b).

Chemical exchange on the timescale of seconds was observed between the NMR signals of the A and B subunits. This interconversion of the A and B conformations could be caused by a disassembly and reassembly of the four-helix bundle, where each subunit has an equal probability of adopting either the A or B conformation. Another plausible model for the exchange process is a sliding of the two-stranded coiled coils relative to each other. In this sliding model, the closely packed A_1B_1 and A_2B_2 coiled coils would not need to dissociate whereas disruption of the less tight inter-coiled-coil packing would allow exchange of the A_1-A_2 and B_1-B_2 interfaces (Figure 5b). The relative movement of the coiled coils boils down to a repositioning of two helical turns. The two models may give rise to different behavior of solvent exchange of the amide protons. A monomeric intermediate is probably (partially) unfolded, similar as has been observed for the helices of the C-terminal domain in the dimeric Mnt(1–76) mutant (Burgering et al., 1994). In that case fast and uniform solvent exchange for the amide protons may be expected. The slow hydrogen–deuterium exchange rates and the observed pattern of amide proton exchange (Figure 7b) seems more consistent with the sliding model. In this model the helices remain largely intact. The amides for which the slowest amide proton exchange rates are observed, Val 66

in particular, remain protected from the solvent, even when the coiled coils stay together but only exchange their relative positions.

Conclusions

We have demonstrated that the structure of the Mnt-C tetramer could be solved combining isotope filtered NMR experiments, symmetric ambiguous distance restraints and modeling. The structure of the tetramerization domain of the Mnt repressor reveals a unique assembly of two right-handed coiled coils. The tetramer is constructed as a dimer of dimers with an overall C_2 symmetry. To date, only two other homo-tetrameric structures have been solved by NMR spectroscopy: the platelet factor 4/IL-8 chimer (Mayo et al., 1995) and the tetramerization domain of p53 (Clore et al., 1995), both with D_2 symmetry. The asymmetric subunit assembly of the Mnt-C peptide and the anti-parallel arrangement of the α-helical subunits facilitated considerably the structure determination of the tetramerization domain of Mnt by NMR spectroscopy. Two sets of resonances that are in slow exchange on the NMR timescale reflect the asymmetric subunit assembly in the four-helix bundle. A relative movement of the two-stranded coiled coils can account for the exchange between the two asymmetric conformations.

Acknowledgements

We thank Carey Waldburger for his help in protein expression and purification and Wijnand Mooij for his initial work on the unlabeled Mnt-C fragment. Rainer Wechselberger is acknowlegded for his assistance in NMR measurements at 750 MHz and Alexandre Bonvin for his support in the structure calculations. This work was supported by the Council of Earth and Life Sciences of the Netherlands Foundation of Scientific Research (NWO/ALW).

References

Amman, E., Brosius, J. and Ptashne, M. (1983) *Gene*, **25**, 167–178.
Bax, A. and Davis, D.G. (1985) *J. Magn. Reson.*, **63**, 207–213.
Bothner-By, A.A., Stephens, R.L., Lee, J., Warren, C.D. and Jeanloz, R.W. (1984) *J. Am. Chem. Soc.*, **106**, 811–813.
Breg, J.N., van Opheusden, J.H.J., Burgering, M.J.M., Boelens, R. and Kaptein, R. (1990) *Nature*, **346**, 586–589.
Brünger, A.T. (1992) *X-PLOR. A system for X-ray Crystallography and NMR*, Yale University Press, New Haven, CT.
Burgering, M.J., Boelens, R., Caffrey, M., Breg, J.N. and Kaptein, R. (1993) *FEBS Lett.*, **330**, 105–109.
Burgering, M.J., Boelens, R., Gilbert, D.E., Breg, J.N., Knight, K.L., Sauer, R.T. and Kaptein, R. (1994) *Biochemistry*, **33**, 15036–15045.
Clore, G.M., Appella, E., Yamada, M., Matsushima, K. and Gronenborn, A.M. (1990) *Biochemistry*, **29**, 1689–1696.
Clore, G.M., Omichinski, J.G., Sakaguchi, K., Zambrano, N., Sakamoto, H., Appella, E. and Gronenborn, A.M. (1995) *Science*, **267**, 1515–1516.
Dayie, K.T. and Wagner, G. (1994) *J. Magn. Reson.*, **A111**, 121–126.
Delaglio, F., Grzesiek, S., Vuister, G.W., Zhu, G., Pfeifer, J. and Bax, A. (1995) *J. Biomol. NMR*, **6**, 277–293.
Düx, P., Whitehead, B., Boelens, R., Kaptein, R. and Vuister, G.W. (1997) *J. Biomol. NMR*, **10**, 301–306.
Fogh, R.H., Schipper, D., Boelens, R. and Kaptein, R. (1995) *J. Biomol. NMR*, **5**, 259–270.
Folkers, P.J.M., Folmer, R.H.A., Konings, R.N.H. and Hilbers, C.W. (1993) *J. Am. Chem. Soc.*, **115**, 3798–3799.
Friedman, A.M., Fischmann, T.O. and Steitz, T.A. (1995) *Science*, **268**, 1721–1727.
Gray, T.M. and Matthews, B.W. (1984) *J. Mol. Biol.*, **175**, 75–81.
Griesinger, C., Otting, G., Wüthrich, K. and Ernst, R.R. (1988) *J. Am. Chem. Soc.*, **110**, 7870–7872.
Jeener, J., Meier, B.H., Bachmann, P. and Ernst, R.R. (1979) *J. Chem. Phys.*, **71**, 4546–4553.
Kabsch, W. and Sander, C. (1983) *Biopolymers*, **22**, 2577–2637.
Kleywegt, G.J., Vuister, G.W., Padilla, A., Knegtel, R.M.A., Boelens, R. and Kaptein, R. (1993) *J. Magn. Reson.*, **B102**, 166–176.
Knight, K.L. and Sauer, R.T. (1988) *Biochemistry*, **27**, 2088–2094.
Knight, K.L., Bowie, J.U., Vershon, A.K., Kelley, R.D. and Sauer, R.T. (1989) *J. Biol. Chem.*, **264**, 3639–3642.
Kohn, W.D., Mant, C.T. and Hodges, R.S. (1997) *J. Biol. Chem.*, **272**, 2583–2586.
Koning, T.G.M., Boelens, R. and Kaptein, R. (1990) *J. Magn. Reson.*, **90**, 111–123.
Koradi, R., Billeter, M. and Wüthrich, K. (1996) *J. Mol. Graph.*, **14**, 52–55.
Laskowski, R.A., MacArthur, M.W., Moss, D.S. and Thornton, J.M. (1993) *J. Appl. Crystallogr.*, **26**, 283–291.
Lee, W., Harvey, T.S., Yin, Y., Yau, P., Litchfield, D. and Arrowsmith, C.H. (1994) *Nat. Struct. Biol.*, **1**, 877–890.
Lupas, A. (1996) *Trends Biochem. Sci.*, **21**, 375–382.
Mayo, K.H., Roongta, V., Ilyina, E., Milius, R. and Barker, S. (1995) *Biochemistry*, **34**, 11399–11409.
Milla, M.E., Brown, B.M. and Sauer, R.T. (1993) *Protein Sci.*, **2**, 2198–2205.
Neri, D., Szyperski, T., Otting, G., Senn, H. and Wüthrich, K. (1989) *Biochemistry*, **28**, 7510–7516.
Nilges, M., Clore, G.M. and Gronenborn, A.M. (1988) *FEBS Lett.*, **239**, 129–136.
Nilges, M. (1993) *Proteins Struct. Funct. Genet.*, **17**, 295–309.
Nooren, I.M.A., Kaptein, R., Sauer, R.T. and Boelens, R. (1999) *Nat. Struct. Biol.*, **6**, 755–759.
O'Donoghue, S.I. and Nilges, M. (1999) In *Biological Magnetic Resonance: Structure, Computation and Dynamics in Protein NMR*, Vol. 17 (Berliner, J.L and Krishna, N.R., Eds.), Plenum, New York, NY, pp. 131–161.
Schulz, G.E. and Schirmer, R.H. (1979) In *Principles of Protein Structure*, Springer-Verlag, New York, NY, pp. 98–101.

Slijper, M., Kaptein, R. and Boelens, R. (1996) *J. Magn. Reson.*, **B111**, 199–203.

Susskind, M.M. and Youderian, P. (1983) In *Lambda II* (Hendrix, R.W., Roberts, J.W., Stahl, F.W. and Weisberg, R., Eds.), Cold Spring Harbor Press, Cold Spring Harbor, NY, pp. 347–366.

Vershon, A.K., Youderain, P., Susskind, M.M. and Sauer, R.T. (1985) *J. Biol. Chem.*, **260**, 12124–12129.

Vis, H., Boelens, R., Mariani, M., Stroop, R., Vorgias, C.E., Wilson, K.S. and Kaptein, R. (1994) *Biochemistry*, **33**, 14858–14870.

Vis, H. Vorgias, C.E., Wilson, K.S., Kaptein, R. and Boelens, R. (1998) *J. Biomol. NMR*, **11**, 265–277.

Waldburger, C.D. and Sauer, R.T. (1995) *Biochemistry*, **34**, 13109–13116.

Wüthrich, K. (1986) *NMR of Proteins and Nucleic Acids*, Wiley, New York, NY.

Zwahlen, C., Legault, P., Vincent, S.J.F., Greenblatt, J., Konrat, R. and Kay, L.E. (1997) *J. Am. Chem. Soc.*, **119**, 6711–6721.